ACS OMEGA

http://pubs.acs.org/journal/acsodf

Article

Phosphorus-Doped Activated Coconut Shell Carbon-Anchored Highly Dispersed Pt for the Chemoselective Hydrogenation of Nitrobenzene to *p*-Aminophenol

Yang Liu, Yao Sheng,* Yuchen Yin, Jiaan Ren, Xinrui Lin, Xiujing Zou,* Xueguang Wang, and Xionggang Lu

Cite This: *ACS Omega* 2022, 7, 11217−11225

Read Online

ACCESS | Metrics & More | Article Recommendations | Supporting Information

ABSTRACT: Highly dispersed Pt nanoparticles (~2.5 nm) on phosphorus-doped activated coconut shell carbon (Pt/P-ACC) were synthesized by a two-step impregnation route. Pt/P-ACC showed a high activity, chemoselectivity, and reusability toward the hydrogenation of nitrobenzene to *p*-aminophenol, with hydrogen as the reducing agent in sulfuric acid. The effects of P species on the catalyst structure, surface properties, and catalytic performance were investigated. It was found that the Pt/P-ACC catalyst had an excellent catalytic activity due to its smaller Pt nanoparticles and higher content of surface-active metal compared with Pt/ACC. Besides, the experimental results and in situ infrared studies demonstrated that the interaction effect between the Pt and P species imbued the surface of Pt with an electron-rich feature, which decreased the adsorption of electron-rich substrates (that is, phenylhydroxylamine) and prevented their full hydrogenation, leading to enhanced selectivity during the hydrogenation of nitrobenzene to *p*-aminophenol.

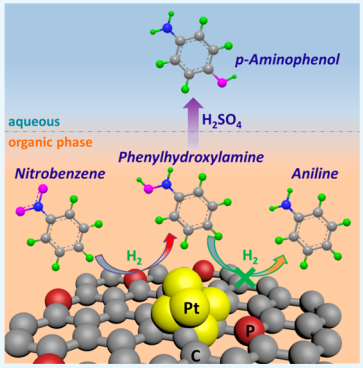

1. INTRODUCTION

p-Aminophenol (PAP) is an important intermediate for the manufacture of analgesic and antipyretic drugs such as acetaminophen, dyestuffs, and photographic chemicals.[1−3] PAP is traditionally obtained by the reduction of phenol, *p*-chloronitrobenzene, or *p*-nitrophenol through iron−acid multistep processes.[4,5] However, these reduction processes have difficulty controlling the reaction rate and produce large amounts of metal sludge, causing poor overall yields and serious environmental pollution. The single-step conversion of nitrobenzene (NB) to PAP over solid metal catalysts in an acid medium is regarded as a sustainable and efficient protocol owing to its low cost and the high-quality product.[6−8] Such a single-step reaction involves the catalytic hydrogenation of NB to phenylhydroxylamine (PHA) and the acid-catalyzed Bamberger rearrangement of PHA (Scheme 1). Meantime, PHA can also be further hydrogenated to aniline (AN), which is the main byproduct.[9,10] In addition, the generated PAP would convert to 4, 4′-diaminodiphenyl ether (DDE), which is very difficult to separate from the PAP because of their similar physicochemical properties.

Generally, supported precious metal catalysts, including Pt, Pd, Au, etc., have been widely investigated for the hydrogenation of NB to PAP in sulfuric acid, and Pt/C is considered as the most promising catalyst owing to its high activity up to now.[11−13] However, Pt catalysts always suffer from a low selectivity to PAP because of the significant full hydrogenation of PHA to form AN. Therefore, developing a Pt catalyst that can catalyze the hydrogenation of NB to PAP with both high activity and high selectivity for PHA is economically appealing and challenging.

For heterogeneous metal catalysts, the metal particle size and the support nature have been demonstrated to influence the catalytic performance for the selective hydrogenation of NB.[14−16] Generally, highly dispersed metal nanoparticles will result in a high catalytic activity, and the electronic properties of metal sites will affect the selectivity of the hydrogenation of the nitro group.[17,18] Recently, surface-modified activated carbon materials, as versatile catalyst supports, have attracted increased interest because of their low cost and excellent chemical stability; additionally, their surface properties can be modulated by heteroatom doping (N, P, S, etc.).[19−21] The doping of phosphorus to carbon materials can enhance the interaction effect between metal sites and support and change the geometrical structure.[22,23]

In the present work, we report a facile method to prepare Pt nanoparticles supported on phosphorus-doped activated coconut shell carbon (Pt/P-ACC) through a two-step impregnation route. The as-prepared Pt/P-ACC catalysts can be used as

Received: January 6, 2022
Accepted: March 8, 2022
Published: March 21, 2022

https://doi.org/10.1021/acsomega.2c00093
ACS Omega 2022, 7, 11217−11225

Scheme 1. Reaction Scheme for the Hydrogenation of NB to PAP

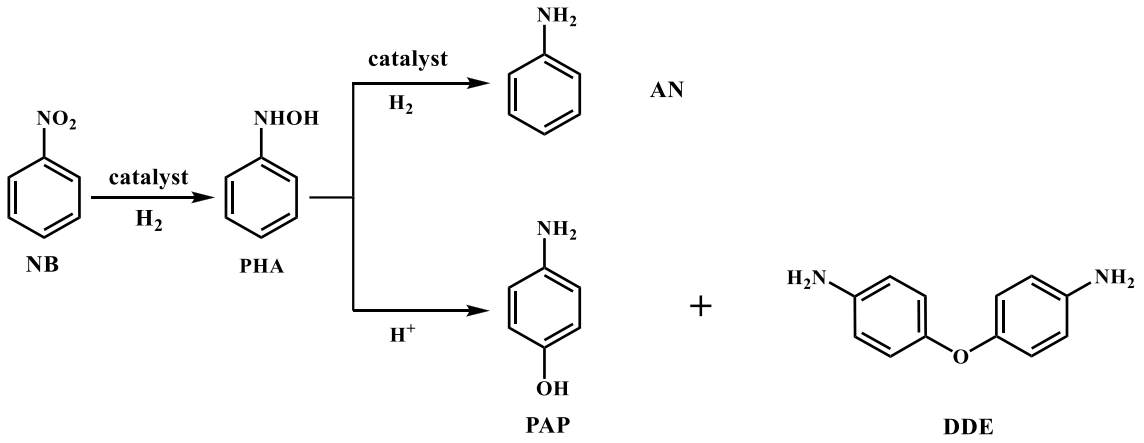

highly efficient heterogeneous catalysts for the hydrogenation of NB to PAP in sulfuric acid using water as the solvent. The effects of surface P species on the catalytic activity and the PAP selectivity were investigated. The adsorption property of PHA on the surface of catalysts was monitored by in situ FTIR, and possible reaction pathways were discussed further.

2. EXPERIMENTAL SECTION

2.1. Materials. The reagent-grade chemicals, such as hexahydrate ($H_2PtCl_6{\cdot}6H_2O$), nitric acid, phytic acid, sulfuric acid, decyltrimethylammonium bromide (C_{10}TAB), dodecyl trimethylammonium bromide (C_{12}TAB), cetyl trimethylammonium bromide (C_{16}TAB), sodium dodecyl benzene sulfonate (SDBS), polyethylene-polypropylene glycol (F127), *N*,*N*-dimethylformamide (DMF), etc., and commercial activated coconut shell carbon (ACC), γ-alumina (γ-Al_2O_3), silica (SiO_2), 3% Pt/C catalyst, 5% Pd/C catalyst, and 5% Ru/C catalyst were all bought from Sinopharm Chemical Reagent Co., Ltd. (Shanghai, China). All supports were treated at high temperature to remove water and impurities before use.

2.2. Preparation of the Catalyst. To remove impurities on the surface of the ACC supports, ACC samples were pretreated as follows: 40 g of ACC, 40 mL of nitric acid, and 400 mL of deionized water were mixed uniformly. The mixture was stirred and refluxed at 80 °C for 8 h, washed with deionized water to neutrality, and dried at 100 °C to obtain ACC supports.

The phosphorus-doped active coconut carbon P-ACC was prepared by the impregnation method. At room temperature, 5 g of treated ACC and appropriate amounts of phytic acid were first dissolved in 30 mL of ethanol and mixed evenly. The mixture was then stirred in a water bath pot at 30 °C for 24 h. The mixture was then stirred at 80 °C, and the ethanol was evaporated slowly. After drying completely, the obtained solids were ground and mixed uniformly. The mixture was then calcined in a high-purity N_2 atmosphere at 500 °C for 3 h with a heating rate of 2 °C min^{-1}. The calcined samples were denoted as *x*P-ACC (*x* = 3, 5, and 7), where *x* represents the mass fraction ratio of phosphorus to ACC.

The 1%Pt/*x*P-ACC catalyst loaded with 1 wt % Pt was prepared by an ultrasonic-assisted impregnation strategy. The typical preparation process is as follows. First, 4 g of the *x*P-ACC powder was dispersed in 160 mL of deionized water and treated under ultrasonic conditions for 10 min. Then, 1.033 mL of a $H_2PtCl_6{\cdot}6H_2O$ aqueous solution with a Pt concentration of 0.2 mol L^{-1} was added to the above mixed solution, and the ultrasonic treatment was continued for 10 min. After this, the mixture was stirred and evaporated at 40 °C. Finally, the solid was directly reduced in a tubular furnace filled with a mixed atmosphere of H_2/N_2 (volume ratio 1:3) and treated at 200 °C for 3 h with a heating rate of 1 °C min^{-1}. For comparison, 1%Pt/ACC, 1%Pt/TiO_2, 1%Pt/γ-Al_2O_3, and 1%Pt/SiO_2 catalysts were also prepared by this method.

2.3. Characterization of the Catalyst. The N_2 adsorption−desorption isotherms were recorded using a Micromeritics ASAP 2020 Sorptometer. Samples were degassed at 200 °C for 8 h and then analyzed at −196 °C. The Brunauer−Emmett−Teller (BET) method was used to calculate and measure the specific surface area of the catalyst. A Bruker D8 Advance diffractometer using Cu Kα radiation (40 kV, 40 mA) was used to record X-ray diffraction (XRD) patterns of all samples. The sample powder was installed in a groove of the sample table, and the scanning range of the 2θ angle was 10−90°. Transmission electron microscopy (TEM) micrographs were obtained by a field emission scanning microscope (JEOL JEM-2010F) operated at 200 kV, and the elements were analyzed by energy-dispersive X-ray spectroscopy (EDX). The surface properties of the catalysts were analyzed by X-ray photoelectron spectroscopy (XPS) using an ESCALAB 250Xi spectrometer equipped with monochromatized Al Kα radiation ($h\nu$ = 1486.6 eV) operated at ca. 1×10^{-9} Torr. The spectra were calibrated using the binding energy of the C 1s peak at 284.6 eV.

The temperature-programmed desorption of hydrogen (H_2-TPD) was carried out on a Biode PCA-140s chemisorption analyzer using H_2 as the probe molecule and a thermal conductivity detector (TCD) as the detector. Typically, 100 mg of the sample was pretreated under an Ar flow at 200 °C for 1 h and reduced in situ under a 10 vol % H_2/Ar flow for 1 h. After it was cooled to 50 °C under an Ar flow, the treated sample was saturated with H_2 and then purged by an Ar flow for 0.5 h to remove the physically adsorbed H_2. Subsequently, the sample was heated to 500 °C at a rate of 10 °C min^{-1} under an Ar flow. The desorption of hydrogen was monitored by TCD.

CO chemisorption was also performed on a Biode PCA-140s chemisorption analyzer. Just like TPD, the catalyst was pretreated and reduced at 200 °C. After the catalyst was cooled to 25 °C with an Ar flow, pulses of 5 vol % CO/Ar were injected into a quartz reactor to carry out the CO

https://doi.org/10.1021/acsomega.2c00093
ACS Omega 2022, 7, 11217−11225

chemisorption analysis. The dispersion of Pt was calculated according to a CO/Pt stoichiometric ratio of 1:1.

2.4. In Situ FTIR Experiments. In situ FTIR spectra were recorded on an in situ FTIR spectrometer (Tensor 27, Bruker) in the range of 2000−1200 cm^{-1} with a resolution of 4 cm^{-1} and 32 scans. Before the test, the in situ cell with a CaF_2 window was heated to 300 °C and held for 0.5 h under vacuum to remove impurities, then cooled to room temperature for loading. First, 20 mg of the sample was pressed and then put into the support plate of the in situ cell. The background spectrum was recorded at 80 °C. Then, PHA was introduced to the sample for adsorption under negative pressure. After the steady state was obtained, the spectrum was collected. NB adsorption was the same as that of PHA. After the steady state was obtained, hydrogen was introduced, and the spectra over time were collected.

2.5. Catalytic Reactions and Product Analyses. All hydrogenation experiments were carried out in 2000 mL round-bottom flasks. PAP was synthesized by the catalytic hydrogenation of NB under sulfuric acid with hydrogen as a hydrogen donor. In a typical experiment, 36 g of NB, an appropriate amount of the catalyst, 0.9 g of C_{12}TAB, 60 mL of concentrated H_2SO_4, and 400 mL of deionized water were uniformly dispersed in the flask. The flask was transferred to a water bath whose temperature had been set to 80 °C with an accuracy of ±1 °C. Before turning on the mechanical stirring, the flask was flushed with N_2 to completely exhaust the air, then hydrogen was continuously injected in the bubbling mode at atmospheric pressure until the end of the reaction. After the reaction was complete, the solution was separated from the reaction mixture for analysis using a filter syringe.

Each reaction was repeated at least three times. The products were analyzed by an Elite HPLC P230p liquid chromatograph equipped with an ultraviolet detector (UV230II) and a high-pressure constant-flow pump (P230II) to determine the conversion and selectivity of the reaction. The high-performance liquid chromatography (HPLC) analysis was performed on a 4.6 mm × 250 mm C_{18} column (Sinochrom ODS-BP 5 μm filler). The product and reactant were detected by a UV detector at λ_{max} = 254 nm using acetonitrile and deionized water (v/v, 70:30) as the mobile phase at a column temperature of 25 °C and flow rate of 1 mL min^{-1} in the isocratic mode.

After the reaction, the used catalyst was filtered, washed with DMF and deionized water, dried at 100 °C, and directly used for the next cycle. Due to the loss of catalyst in the recovery process, the amount of the catalyst changed in each subsequent cycle; however, the 1%Pt/5P-ACC/NB/sulfuric acid/C_{12}TAB/deionized water ratio and the reaction conditions were always the same as those in the first reaction.

3. RESULTS AND DISCUSSION

3.1. Physical and Chemical Properties of the Pt/P-ACC Catalysts. The actual Pt loading and P contents in the as-prepared materials were determined by ICP-AES and XPS, and the data are summarized in Table 1. For all Pt-based samples, the bulk Pt contents measured by ICP were all located at 1.0 ± 0.05 wt %, which was consistent with the surface content of Pt in the 1%Pt/ACC. However, for 1%Pt/*x*P-ACC the surface Pt contents on catalysts obtained by XPS first increased and then declined with the increases content of P and exhibited a maximum at 1%Pt/5P-ACC. This result implied that the addition of P improved the surface concentration of Pt on the 1%Pt/*x*P-ACC catalyst. In addition, all the 1%Pt/*x*P-ACC catalysts showed a decline in their specific surface areas compared with that of ACC because of the incorporation of P and Pt.

Table 1. P and Pt Contents and Physical Properties of the Catalysts

	Pt (wt %)					
catalyst	bulk[a]	surface[b]	P (wt %)[b]	Pt dispersion (%)	surface areas (m^2 g^{-1})[c]	particle size (nm)
ACC					1103	
P-ACC			5.21		940	
1%Pt/ACC	0.98	1.09		33	852	4.3
1%Pt/3P-ACC	1.03	1.40	2.20	40	820	3.7
1%Pt/5P-ACC	1.05	2.31	3.33	56	818	2.5
1%Pt/7P-ACC	0.99	1.84	5.45	47	752	3.1
1%Pt/TiO_2	0.94	0.98		27	118	5.5
1%Pt/γ-Al_2O_3	0.97	0.90		29	418	5.3
1%Pt/SiO_2	1.01	0.99		21	266	6.4
spent 1% Pt/5P-ACC	1.04	2.25	3.30	55	804	2.5

[a]Determined by ICP. [b]Determined by XPS. [c]Determined by BET.

Figure 1a presents the XRD patterns of the P-ACC, 1%Pt/ACC, and 1%Pt/*x*P-ACC (*x* = 3, 5, 7) materials. The characteristic peaks of graphitic carbon at ∼23° and ∼43° were observed in all samples.[24−26] 1%Pt/ACC showed a typical diffraction peak at 2θ of 39.8°, which is characteristic of metal Pt. The intensity of the Pt peak gradually weakened as the content of P increased, and no observable diffraction ascribed to the Pt species in 1%Pt/5P-ACC and 1%Pt/7P-ACC could be detected, indicating its good dispersion and small particle size. TEM images in Figure 1b−e demonstrate that the metallic nanoparticles of both 1%Pt/ACC and 1%Pt/*x*P-ACC were homogeneously dispersed on the carbon support without obvious agglomeration. However, the particle size of Pt on 1% Pt/ACC was 4.3 nm, which is larger than those on 1%Pt/*x*P-ACC and in agreement with the XRD results. This could possibly be explained by the uniformly distributed defects in the carbon lattice induced by P doping providing anchor sites for the nucleation of Pt,[27,28] resulting in the uniform dispersion of Pt nanoparticles. In addition, P doping introduced negatively charged electron-rich donors on the carbon surface, which can lead to a higher local electron density, enhance the reduction of $PtCl_6^{2-}$, and promote the high dispersion of Pt nanoparticles.[27,29] However, the surface areas of the samples decreased with the increased content of P (Table 1), which was not conducive to the dispersion of metal particles. Therefore, 1%Pt/5P-ACC with the optimum P content had the smallest particle size of 2.5 nm. The existence state of the Pt species on the P-ACC was further investigated by XPS analysis. Furthermore, the EDS elemental mapping images, which suggest the uniform distribution of the P and Pt species of 1%Pt/5P-ACC, are shown in Figure 1f.

The XPS analysis was used to identify the surface electronic state and the composition of the as-synthesized materials. Figure 2a shows the Pt 4f XPS spectra of 1%Pt/ACC and 1%

https://doi.org/10.1021/acsomega.2c00093
ACS Omega 2022, 7, 11217−11225

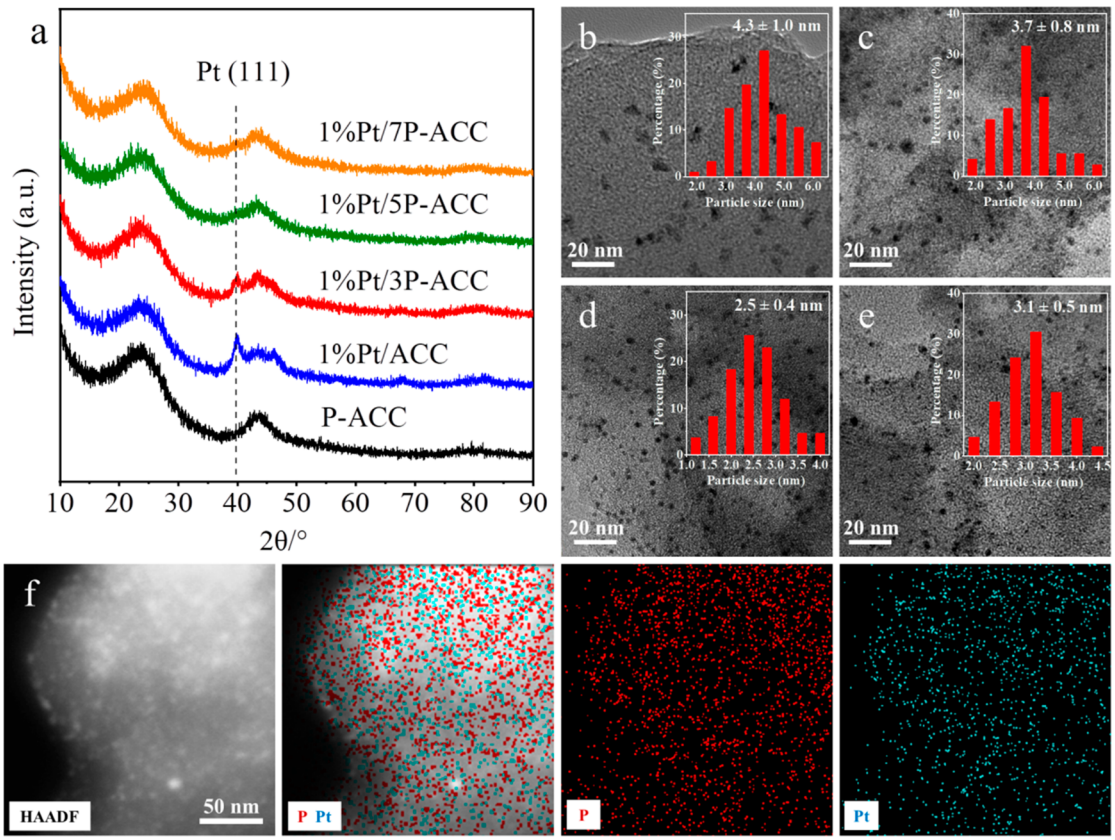

Figure 1. (a) XRD patterns of P-ACC, 1%Pt/ACC, and 1%Pt/*x*P-ACC. TEM images of (b) 1%Pt/ACC, (c) 1%Pt/3P-ACC, (d) 1%Pt/5P-ACC, and (e) 1%Pt/7P-ACC. (f) HAADF-STEM image of 1%Pt/5P-ACC and elemental mapping images of Pt and P.

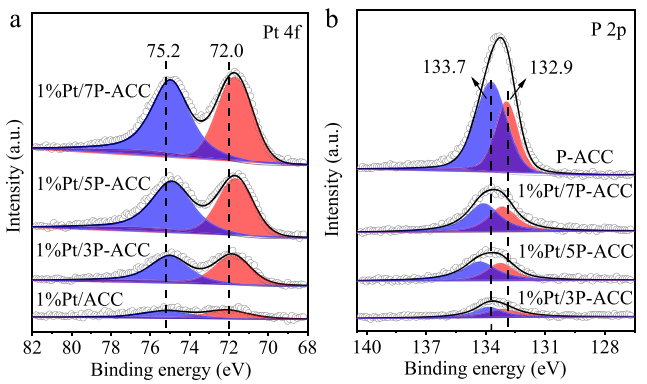

Figure 2. (a) Pt 4f XPS spectra of the 1%Pt/ACC and 1%Pt/*x*P-ACC samples. (b) P 2p XPS spectra of the P-ACC, 1%Pt/ACC, and 1%Pt/*x*P-ACC samples.

Pt/*x*P-ACC (x = 3, 5, 7). For 1%Pt/ACC, two relatively symmetric binding energy curves with peaks at 72.0 and 75.2 eV were characteristic of Pt^0,[30−32] which indicated the Pt species exist dominantly in reduced forms. It is obvious that the intensity of the Pt 4f spectrum of 1%Pt/ACC is much lower than those of 1%Pt/*x*P-ACC. The intensity of the surface Pt signal for 1%Pt/*x*P-ACC increased significantly and then tended toward a steady-state value, suggested that the concentration of surface metallic Pt species gradually increased with the P content. TEM, XRD, and XPS results demonstrated that the highly dispersed Pt nanoparticles with a high surface Pt^0 concentration on the P-ACC support were formed, which was the primary reason for the enhanced hydrogenation activity of 1%Pt/*x*P-ACC. Furthermore, the Pt 4f spectra for 1%Pt/*x*P-ACC showed a negative shift when compared with that of 1%Pt/ACC, which confirmed the strong electron interactions between Pt and P. In the corresponding P 2p spectra of P-ACC and 1%Pt/*x*P-ACC (Figure 2b), the two main peaks with binding energies at approximately 132.9 and 133.7 eV were assigned to P−C and P−O bonds,[28,33−35] respectively. The negative shift of the Pt 4f peak and the positive shift of the P 2p peak of 1%Pt/*x*P-ACC confirmed the interaction between Pt and P. This is attributed to the introduction of negatively charged electron-rich donors on the carbon surface by P doping, resulting in electron transfer from P-ACC to Pt and a richer electron density of Pt[27,36,37] that influenced the catalytic selectivity of the Pt catalysts, as discussed later.

H_2-TPD was carried out to investigate the effect of P on the adsorption behavior of hydrogen on the catalyst's surface and the interaction of Pt and P. As shown in Figure 3, no distinct peak from P-ACC was observed due to the poor chemisorption ability of hydrogen. The peak at ca. 315 °C was attributed to chemisorbed hydrogen, and its peak areas followed the order 1%Pt/ACC < 1%Pt/3P-ACC < 1%Pt/7P-ACC < 1%Pt/5P-ACC. This order can be ascribed to the increased amount of exposed Pt in 1%Pt/*x*P-ACC from CO chemisorption (Table 1), suggesting the great capacity of the surfaces of the P-doped catalysts to activate H_2 compared to those of the the undoped P catalysts. Meanwhile, the hydrogen desorption peaks of 1% Pt/*x*P-ACC showed a slight shift toward the higher temperature region (322−335 °C) compared with those of the 1%Pt/ACC, indicating the interaction between Pt and P. Moreover, a high-temperature TPD peak (ca. 458 °C), the hydrogen

https://doi.org/10.1021/acsomega.2c00093
ACS Omega 2022, 7, 11217−11225

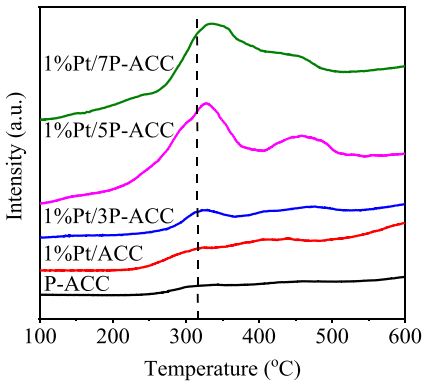

Figure 3. H_2-TPD profiles of the 1%Pt/ACC and 1%Pt/*x*P-ACC samples.

spillover,[38] was noticed on the 1%Pt/*x*P-ACC samples, with a maximum for 1%Pt/5P-ACC. This implied that highly dispersed Pt was necessary to facilitate the transfer of active hydrogen, which allowed the hydrogenation reaction to proceed more rapidly.

3.2. Catalytic Performance. Figure 4a shows the NB conversion and product selectivity versus the reaction time

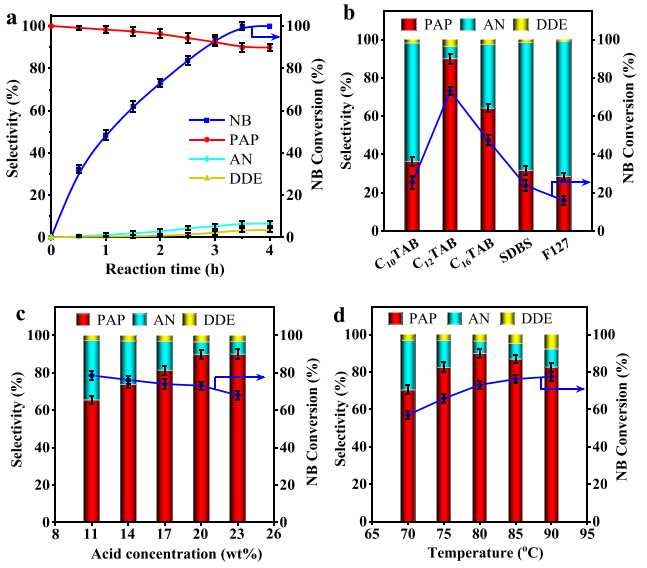

Figure 4. Effects of (a) the reaction time, (b) the surfactant, (c) the acid concentration, and (d) the temperature on the hydrogenation of NB to PAP using the 1%Pt/5P-ACC catalyst.

profile for the hydrogenation of NB to PAP with H_2 at atmospheric pressure in a mixture of NB and a 20 wt % sulfuric acid aqueous solution. It is clear that the selectivity to DDE began to increase dramatically when the conversion of NB was more than 60% because the high concentration of generated PAP might have converted to DDE. Besides, the selectivity of AN increased as the reaction proceeded, while the PAP selectivity decreased slightly but it was still high than 89% with full NB conversion. The was because the generated AN reduced the overall acidity of the solution and thus decreased the rate of the acid-catalyzed Bamberger rearrangement of PHA. In addition, the effects of the surfactant, the acid concentration, and the reaction temperature were explored, and the results are displayed in Figure 4b–d, respectively. In order to provide an intuitive understanding of the product yield, all the product selectivities were obtained by prolonging the reaction period until 100% conversion was achieved. Since the hydrogenation of NB occurred in the organic phase while the rearrangement of PHA occurred in an aqueous solution of sulfuric acid, the catalytic activity and selectivity depended on whether NB could adsorb to the catalyst surface and whether PHA could successfully diffuse into the aqueous solution. Figure 4b shows the influence of surfactants on the reaction rate and the PAP selectivity. It appears that adding the cationic surfactants (C_{10}TAB, C_{12}TAB, and C_{16}TAB) led to higher NB conversions and PAP selectivities compared to adding the anionic surfactant (SDBS) or the nonionic surfactant (F127). Among these cationic surfactants, C_{12}TAB with an appropriate chain length not only increased the degree of dispersion of NB in water but also ensured that the PHA could desorb from the catalyst surface. Given that an acid is necessary for the rearrangement of PHA to PAP, otherwise aniline would be the only product, the effect of the acid concentration on the NB conversion and the PAP selectivity was investigated, and the results are shown in Figure 4c. A continuous increase of the PAP selectivity from 65.8% to 90.0% with a slight decrease in the NB conversion was achieved when the acid concentration was increased. Considering that the PAP selectivity remained nearly constant at a higher acid concentration, an acid concentration of 20 wt % was chosen as the optimum for the hydrogenation of NB. Moreover, the reaction temperature had a significant influence on the catalytic performance, and the results are displayed in Figure 4d. As the reaction temperature increased from 70 to 80 °C, the NB conversion gradually increased from 57.0% to 73.1% and the PAP selectivity increased from 70.4% to 89.9%, respectively. When the reaction temperature was further increased from 80 to 90 °C, the NB conversion increased continuously from 73.1% to 77.5% while the selectivity to PAP decreased from 89.9% to 82.6%, respectively. This might be because the increased reaction temperature accelerated both the hydrogenation of NB and the rearrangement reaction of PHA. However, the conversion of PAP to DDE would be remarkably increased at a higher reaction temperature (>80 °C), resulting in a decrease in the PAP selectivity.

The catalytic performances of various catalysts for the hydrogenation of NB to PAP are summarized in Table 2. It is noteworthy that the support nature of the Pt catalysts strongly influences the activity and the PAP selectivity. The blank P-ACC support had no activity for the NB hydrogenation, and the rate achieved on Pt/ACC was higher than those on other Pt catalysts such as Pt/TiO_2, Pt/γ-Al_2O_3, and Pt/SiO_2 (entries 2 and 6–8, respectively). When P species were introduced, the Pt/*x*P-ACC catalysts exhibited enhanced catalytic activities compared with that of Pt/ACC, which was due to the smaller Pt nanoparticle size and the increased amount of exposed Pt in Pt/*x*P-ACC. The NB conversion first increased and then decreased with the increased P content and reached a maximum of 73.1% for the Pt/5P-ACC catalyst (entries 3–5). However, the PAP selectivity continued increased from 45.2% to 90.2% with the increasing P content and remained nearly constant for Pt/5P-ACC and Pt/7P-ACC. These variations of the PAP selectivity matched well with the shift trend of the binding energy from XPS results, indicating that the PAP selectivity is closely related to the surface electronic structure of Pt. The excellent catalytic performances of Pt/*x*P-ACC were not only significantly higher than those of

https://doi.org/10.1021/acsomega.2c00093
ACS Omega 2022, 7, 11217–11225

Table 2. Hydrogenation of NB to PAP over Different Catalysts[a]

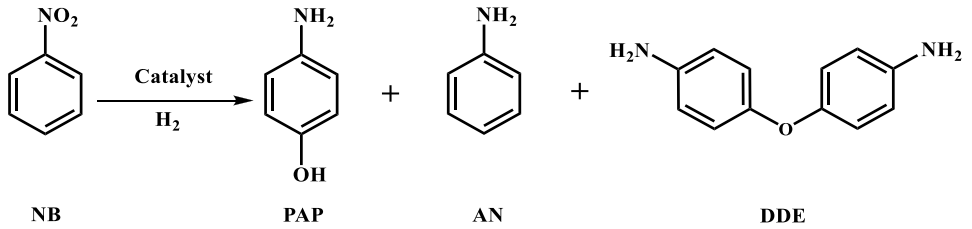

entry	catalyst	conversion[b] (%)	product selectivity[c] (%)		
			PAP	AN	DDE
1	P-ACC	0			
2	1%Pt/ACC	37.0	45.2	52.9	1.9
3	1%Pt/3P-ACC	43.2	78.5	18.5	3.0
4	1%Pt/5P-ACC	73.1	89.9	6.6	3.5
5	1%Pt/7P-ACC	64.0	90.2	6.1	3.7
6	1%Pt/TiO_2	18.7	38.3	60.3	1.7
7	1%Pt/γ-Al_2O_3	24.7	42.3	55.7	2.0
8	1%Pt/SiO_2	15.1	25.4	73.5	1.1
9	3%Pt/C	34.0	31.7	67.0	1.3
10	5%Pd/C	21.4	22.0	77.1	0.9
11	5%Ru/C	13.0	18.4	80.8	0.8

[a]Reaction conditions are as follows: 292 mmol NB, [NB]/[metal] = 9512 (mol mol^{-1}), 400 mL of deionized water, 60 mL of H_2SO_4, and 0.9 g of C_{12}TAB at 80 °C. The reducing agent was H_2 under atmospheric pressure. [b]Conversion at 2 h. [c]Selectivity at 100% conversion of NB.

Table 3. Comparison of Different Reported Catalysts for This Reaction

catalyst	reaction conditions[a]	n_{NB}/n_{metal}	conversion (%)	PAP selectivity (%)	ref
0.5%Pt@HZSM-5	1 MPa H_2, 130 °C, 3 h	253	100	75.0	39
2%Pt/ZrO_2	1 MPa H_2, 80 °C, 8 h	2853	86.7	88.1	40
Pt/FSAPO-5	0.9 MPa H_2, 150 °C	5707	100	53.2	41
1%Au/TiO_2	1 MPa H_2, 100 °C, 4 h	951	78.0	81.0	12
3%Pt/C	0.1 MPa H_2, 80 °C, 3 h	2987	41.0	26.0	42
0.015%Pt−Pb/MgAPO-5	0.4 MPa H_2, 165 °C, 2 h	4227	100	75.5	43
1%Pt/5P-ACC	H_2, atmospheric pressure, 80 °C, 3.5 h	9512	100	89.9	this work

[a]Adapted as the optimal performance was observed.

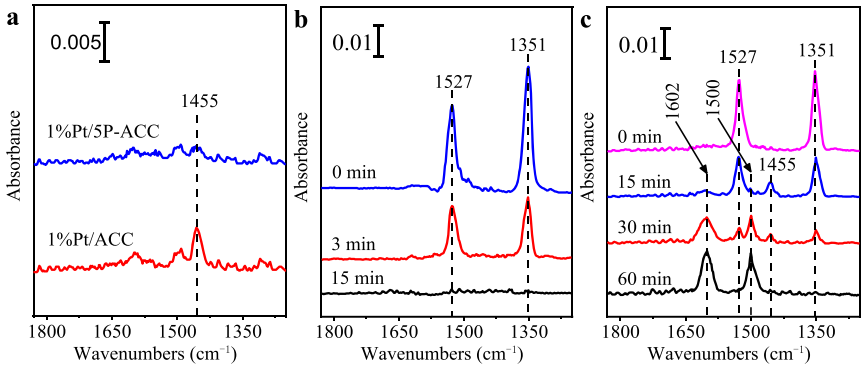

Figure 5. (a) FTIR spectra of adsorbed PHA species on 1%Pt/ACC and 1%Pt/5P-ACC. In situ FTIR spectra of adsorbed NB species on (b) 1% Pt/5P-ACC and (c) 1%Pt/ACC at 80 °C as a function of time in a flow of H_2.

commercial noble metals catalysts, such as Pd/C, Pt/C, and Ru/C (entries 9−11, respectively), but also surpassed those of various noble metal catalysts reported for the hydrogenation of NB to PAP under similar reaction conditions (Table 3).[39−43]

To further explain the enhanced selectivity for the hydrogenation of NB to PAP, the adsorption properties of PHA on different catalyst surfaces and the hydrogenation process of NB were investigated by in situ FTIR spectroscopy. As shown in Figure 5a, when PHA was adsorbed on 1%Pt/ACC and 1%Pt/5P-ACC at 80 °C, the vibration bands at ca. 1455 cm^{-1} corresponding to PHA could be observed on 1%Pt/ACC.[44,45] No obvious adsorption of PHA occurred on 1%Pt/5P-ACC, indicating that the adsorption of PHA onto 1%Pt/5P-ACC was restrained when the P atoms were introduced. Then, the catalyst disk was heated in a N_2 flow at 200 °C for 30 min, followed by the adsorption of NB at 80 °C. As shown

https://doi.org/10.1021/acsomega.2c00093
ACS Omega 2022, 7, 11217−11225

in Figure 5b and c, the vibration bands at ca. 1527 and 1351 cm^{-1} corresponding to the nitro group can be observed for both 1%Pt/ACC and 1%Pt/5P-ACC (t = 0 min),[44,46] respectively, suggesting that NB interacts with the catalyst surface through the nitro group. When flowing H_2 (atmospheric pressure) was introduced to the catalyst disk, the reactivity of the adsorbed NB species was studied by time-resolved in situ FTIR. Figure 5b shows that the intensity of the band due to nitro groups on 1%Pt/5P-ACC decreased after 3 min and disappeared at t = 15 min. In contrast, the nitro groups still existed on the 1%Pt/ACC catalyst surface after 30 min due to its comparably low activity (Figure 5c). Additionally, as shown in Figure 5c, 1%Pt/ACC showed a new band assignable to PHA at 1455 cm^{-1}, which appeared and gradually decreased after 15 min. Then, new bands due to adsorbed AN (FTIR bands at 1602 and 1500 cm^{-1}) appeared, and their intensity increased with time.[47] However, no obvious signals for PHA and AN were observed for 1%Pt/5P-ACC during the hydrogenation of NB. Based on the above FTIR adsorption results, we can conclude that the adsorption properties of PHA in the active catalytic sites can determine the chemoselectivity during the hydrogenation of NB to PAP.

The stability and reusability of 1%Pt/5P-ACC catalyst was investigated. After the reaction, the catalyst was recovered by simple filtration, then washed with ethanol and dried at 100 °C. As shown in Figure 6, the catalytic activity and the PAP

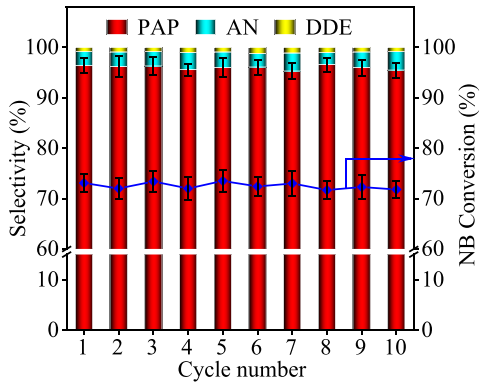

Figure 6. Reusable profiles of 1%Pt/5P-ACC for the hydrogenation of NB to PAP. Reaction conditions are as follows: 292 mmol NB, [NB]/[metal] = 9512 (mol mol^{-1}), 400 mL of deionized water, 60 mL of H_2SO_4, and 0.9 g of C_{12}TAB at 80 °C for 2 h. The reducing agent was H_2 under atmospheric pressure.

selectivity were almost unchanged at ∼73% and 96%, respectively, even when the catalyst was used 10 times, indicating its high stability. Though the corrosion of the catalyst under such harsh condition has always been reported in previous studies, the XRD (Figure S1a), TEM (Figure S1b), XPS (Figure S1c and d), and ICP (Table 1) analyses revealed that the crystalline phase, the Pt particle size, the chemical state, even the Pt content were retained in spent 1%Pt/5P-ACC. These results indicated that 1%Pt/5P-ACC was highly stable and reusable for the hydrogenation of NB to PAP.

4. CONCLUSIONS

In conclusion, we have reported that highly dispersed Pt nanoparticles supported on phosphorus-doped activated coconut shell carbon are highly active and selective for the hydrogenation of NB to PAP. The superior activity of Pt/P-ACC can be attributed to the smaller nanoparticle size and the higher surface active metal content compared to those of the Pt/ACC. The interaction between the Pt and P species made the surface of Pt highly electron-rich, which decreased the adsorption of phenylhydroxylamine and prevented its full hydrogenation, leading to the enhanced PAP selectivity. Moreover, Pt/P-ACC is highly stable and can be reused for the hydrogenation of NB to PAP in sulfuric acid without a decrease in the catalytic efficiency.

■ ASSOCIATED CONTENT

Supporting Information

The Supporting Information is available free of charge at https://pubs.acs.org/doi/10.1021/acsomega.2c00093.

XRD pattern, TEM image, and XPS spectra of spent 1% Pt/5P-ACC (PDF)

■ AUTHOR INFORMATION

Corresponding Authors

Yao Sheng − *State Key Laboratory of Advanced Special Steel, School of Materials Science and Engineering, Shanghai University, Shanghai 20444, China;* orcid.org/0000-0003-0609-8929; Email: shengyao@shu.edu.cn

Xiujing Zou − *State Key Laboratory of Advanced Special Steel, School of Materials Science and Engineering, Shanghai University, Shanghai 20444, China*; Email: xjzou@shu.edu.cn

Authors

Yang Liu − *State Key Laboratory of Advanced Special Steel, School of Materials Science and Engineering, Shanghai University, Shanghai 20444, China*

Yuchen Yin − *State Key Laboratory of Advanced Special Steel, School of Materials Science and Engineering, Shanghai University, Shanghai 20444, China*

Jiaan Ren − *State Key Laboratory of Advanced Special Steel, School of Materials Science and Engineering, Shanghai University, Shanghai 20444, China*

Xinrui Lin − *State Key Laboratory of Advanced Special Steel, School of Materials Science and Engineering, Shanghai University, Shanghai 20444, China*

Xueguang Wang − *State Key Laboratory of Advanced Special Steel, School of Materials Science and Engineering, Shanghai University, Shanghai 20444, China;* orcid.org/0000-0001-5123-2483

Xionggang Lu − *State Key Laboratory of Advanced Special Steel, School of Materials Science and Engineering, Shanghai University, Shanghai 20444, China*

Complete contact information is available at: https://pubs.acs.org/10.1021/acsomega.2c00093

Notes

The authors declare no competing financial interest.

■ ACKNOWLEDGMENTS

This research was supported by National Natural Science Foundation of China (U1860203).

■ REFERENCES

(1) Fu, L.; Zhou, W.; Wen, M.; Wu, Q.; Li, W.; Wu, D.; Zhu, Q.; Ran, J.; Ren, P. Layered CuNi-Cu_2O/$NiAlO_x$ Nanocatalyst for Rapid

Conversion of *p*-Nitrophenol to *p*-Aminophenol. *Nano Res.* **2021**, *14*, 4616−4624.
(2) Yu, Y.; Jung, E.; Kim, H. J.; Cho, A.; Kim, J.; Yu, T.; Lee, J. Protein Particles Decorated with Pd Nanoparticles for the Catalytic Reduction of *p*-Nitrophenol to *p*-Aminophenol. *ACS Appl. Nano Mater.* **2020**, *3*, 10487−10496.
(3) Swathy, T. S.; Jinish Antony, M.; George, N. Active Solvent Hydrogen-Enhanced *p*-Nitrophenol Reduction Using Heterogeneous Silver Nanocatalysts@Surface-Functionalized Multiwalled Carbon Nanotubes. *Ind. Eng. Chem. Res.* **2021**, *60*, 7050−7064.
(4) Rode, C. V.; Vaidya, M. J.; Chaudhari, R. V. Synthesis of *p*-Aminophenol by Catalytic Hydrogenation of Nitrobenzene. *Org. Process Res. Dev.* **1999**, *3*, 465−470.
(5) Kelly, S. M.; Lipshutz, B. H. Chemoselective Reductions of Nitroaromatics in Water at Room Temperature. *Org. Lett.* **2014**, *16*, 98−101.
(6) Nadgeri, J. M.; Biradar, N. S.; Patil, P. B.; Jadkar, S. T.; Garade, A. C.; Rode, C. V. Control of Competing Hydrogenation of Phenylhydroxylamine to Aniline in a Single-Step Hydrogenation of Nitrobenzene to *p*-Aminophenol. *Ind. Eng. Chem. Res.* **2011**, *50*, 5478−5484.
(7) Zhang, T.; Jiang, J.; Wang, Y. Green Route for the Preparation of *p*-Aminophenol from Nitrobenzene by Catalytic Hydrogenation in Pressurized CO_2/H_2O System. *Org. Process Res. Dev.* **2015**, *19*, 2050−2054.
(8) Wang, T.; Dong, Z.; Cai, W.; Wang, Y.; Fu, T.; Zhao, B.; Peng, L.; Ding, W.; Chen, Y. An Efficient Hydrogenation Catalyst in Sulfuric Acid for the Conversion of Nitrobenzene to *p*-Aminophenol: N-Doped Carbon with Encapsulated Molybdenum Carbide. *Chem. Commun.* **2016**, *52*, 10672−10675.
(9) Liu, S.; Hao, Y.; Jiang, J. Bamberger Rearrangement of N-Arylhydroxylamine to *p*-Aminophenol in a CO_2-H_2O System. *Ind. Eng. Chem. Res.* **2014**, *53*, 8372−8375.
(10) Joncour, R.; Ferreira, A.; Duguet, N.; Lemaire, M. Preparation of para-Aminophenol from Nitrobenzene through Bamberger Rearrangement Using a Mixture of Heterogeneous and Homogeneous Acid Catalysts. *Org. Process Res. Dev.* **2018**, *22*, 312−320.
(11) Liu, Y.; Fang, Y.; Lu, X.; Wei, Z.; Li, X. Hydrogenation of Nitrobenzene to *p*-Aminophenol Using Pt/C Catalyst and Carbon-Based Solid Acid. *Chem. Eng. J.* **2013**, *229*, 105−110.
(12) Zou, L.; Cui, Y.; Dai, W. Highly Efficient Au/TiO_2 Catalyst for One-Pot Conversion of Nitrobenzene to *p*-Aminophenol in Water Media. *Chin. J. Chem.* **2014**, *32*, 257−262.
(13) Zhang, T.; Jiang, J.; Wang, Y. Supported Bimetallic Catalyst Pt-Pb/SiO_2 for Selective Conversion of Nitrobenzene to *p*-Aminophenol in Pressurized CO_2/H_2O System. *Chin. Chem. Lett.* **2017**, *28*, 307−311.
(14) Lakshminarayana, B.; Satyanarayana, G.; Subrahmanyam, C. Bimetallic Pd-Au/TiO_2 Nanoparticles: An Efficient and Sustainable Heterogeneous Catalyst for Rapid Catalytic Hydrogen Transfer Reduction of Nitroarenes. *ACS omega* **2018**, *3*, 13065−13072.
(15) Zhang, Q.; Bu, J.; Wang, J.; Sun, C.; Zhao, D.; Sheng, G.; Xie, X.; Sun, M.; Yu, L. Highly Efficient Hydrogenation of Nitrobenzene to Aniline over Pt/CeO_2 Catalysts: The Shape Effect of the Support and Key Role of Additional Ce^{3+} Sites. *ACS Catal.* **2020**, *10*, 10350−10363.
(16) Hu, Z.; Liang, J.; Ding, K.; Ai, Y.; Liang, Q.; Sun, H. Insight into the Selectivity of Nano-Catalytic Nitroarenes Reduction over Other Active Groups by Exploring Hydrogen Sources and Metal Components. *Appl. Catal., A* **2021**, *626*, 118339.
(17) Chatterjee, S.; Bhattacharya, S. K. Size-Dependent Catalytic Activity of PVA-Stabilized Palladium Nanoparticles in *p*-Nitrophenol Reduction: Using a Thermoresponsive Nanoreactor. *ACS omega* **2021**, *6*, 20746−20757.
(18) Chen, G.; Xu, C.; Huang, X.; Ye, J.; Gu, L.; Li, G.; Tang, Z.; Wu, B.; Yang, H.; Zhao, Z.; Zhou, Z.; Fu, G.; Zheng, N. Interfacial Electronic Effects Control the Reaction Selectivity of Platinum Catalysts. *Nat. Mater.* **2016**, *15*, 564−569.
(19) Zhang, L.; Liu, X.; Zhou, X.; Gao, S.; Shang, N.; Feng, C.; Wang, C. Ultrafine Pd Nanoparticles Anchored on Nitrogen-Doping Carbon for Boosting Catalytic Transfer Hydrogenation of Nitroarenes. *ACS Omega* **2018**, *3*, 10843−10850.
(20) Pentsak, E. O.; Galushko, A. S.; Cherepanova, V. A.; Ananikov, V. P. How to Make a Cocktail of Palladium Catalysts with Cola and Alcohol: Heteroatom Doping vs. Nanoscale Morphology of Carbon Supports. *Nanomaterials* **2021**, *11*, 2599.
(21) Lu, C.; Zhu, Q.; Zhang, X.; Ji, H.; Zhou, Y.; Wang, H.; Liu, Q.; Nie, J.; Han, W.; Li, X. Decoration of Pd Nanoparticles with N and S Doped Carbon Quantum Dots as a Robust Catalyst for the Chemoselective Hydrogenation Reaction. *ACS Sustainable Chem. Eng.* **2019**, *7*, 8542−8553.
(22) Rangraz, Y.; Heravi, M. M.; Elhampour, A. Recent Advances on Heteroatom-Doped Porous Carbon/Metal Materials: Fascinating Heterogeneous Catalysts for Organic Transformations. *Chem. Rec.* **2021**, *21*, 1985−2073.
(23) Chen, X.; Shen, Q.; Li, Z.; Wan, W.; Chen, J.; Zhang, J. Metal-Free H_2 Activation for Highly Selective Hydrogenation of Nitroaromatics Using Phosphorus-Doped Carbon Nanotubes. *ACS Appl. Mater. Interfaces* **2020**, *12*, 654−666.
(24) Sankar, S.; Ahmed, A. T. A.; Inamdar, A. I.; Im, H.; Im, Y. B.; Lee, Y.; Kim, D. Y.; Lee, S. Biomass-Derived Ultrathin Mesoporous Graphitic Carbon Nanoflakes as Stable Electrode Material for High-Performance Supercapacitors. *Mater. Design* **2019**, *169*, 107688.
(25) Qiu, Q.; Zhou, M.; Cai, W.; Zhou, Q.; Zhang, Y.; Wang, W.; Liu, M.; Liu, J. A Comparative Investigation on Direct Carbon Solid Oxide Fuel Cells Operated with Fuels of Biochar Derived from Wheat Straw, Corncob, and Bagasse. *Biomass and bioenergy* **2019**, *121*, 56−63.
(26) Sheng, Y.; Wang, X.; Xing, Z.; Chen, X.; Zou, X.; Lu, X. Highly Active and Chemoselective Reduction of Halogenated Nitroarenes Catalyzed by Ordered Mesoporous Carbon Supported Platinum Nanoparticles. *ACS Sustainable Chem. Eng.* **2019**, *7*, 8908−8916.
(27) Zhu, J.; He, G.; Liang, L.; Wan, Q.; Shen, P. Direct Anchoring of Platinum Nanoparticles on Nitrogen and Phosphorus-Dual-Doped Carbon Nanotube Arrays for Oxygen Reduction Reaction. *Electrochim. Acta* **2015**, *158*, 374−382.
(28) Song, P.; Zhu, L.; Bo, X.; Wang, A.; Wang, G.; Guo, L. Pt Nanoparticles Incorporated into Phosphorus-Doped Ordered Mesoporous Carbons: Enhanced Catalytic Activity for Methanol Electrooxidation. *Electrochim. Acta* **2014**, *127*, 307−314.
(29) Wang, C.; Hu, F.; Yang, H.; Zhang, Y.; Lu, H.; Wang, Q. 1.82 wt.% Pt/N, P Co-Doped Carbon Overwhelms 20 wt.% Pt/C as a High-Efficiency Electrocatalyst for Hydrogen Evolution Reaction. *Nano Res.* **2017**, *10*, 238−246.
(30) Chen, H.; Zhang, R.; Bao, W.; Wang, H.; Wang, Z.; Wei, Y. Effective Catalytic Abatement of Indoor Formaldehyde at Room Temperature over TS-1 Supported Platinum with Relatively Low Content. *Catal. Today* **2020**, *355*, 547−554.
(31) Wang, L.; Tang, R.; Kheradmand, A.; Jiang, Y.; Wang, H.; Yang, W.; Chen, Z.; Zhong, X.; Ringer, S. P.; Liao, X.; Liang, W.; Huang, J. Enhanced Solar-Driven Benzaldehyde Oxidation with Simultaneous Hydrogen Production on Pt Single-Atom Catalyst. *Appl. Catal., B* **2021**, *284*, 119759.
(32) Chen, Q.; Yu, C.; Li, H.; He, Z.; Liu, J. Composition Modulation of Pt-Based Nanowire Electrocatalysts Enhances Methanol Oxidation Performance. *Inorg. Chem.* **2020**, *59*, 1376−1382.
(33) Patel, M. A.; Luo, F.; Khoshi, M. R.; Rabie, E.; Zhang, Q.; Flach, C. R.; Mendelsohn, R.; Garfunkel, E.; Szostak, M.; He, H. P-Doped Porous Carbon as Metal Free Catalysts for Selective Aerobic Oxidation with an Unexpected Mechanism. *ACS Nano* **2016**, *10*, 2305−2315.
(34) Zhang, B.; Yang, F.; Liu, X.; Wu, N.; Che, S.; Li, Y. Phosphorus Doped Nickel-Molybdenum Aerogel for Efficient Overall Water Splitting. *Appl. Catal., B* **2021**, *298*, 120494.
(35) Li, Y.; Liu, Y.; Wang, M.; Xu, X.; Lu, T.; Sun, C.; Pan, L. Phosphorus-Doped 3D Carbon Nanofiber Aerogels Derived from

https://doi.org/10.1021/acsomega.2c00093
ACS Omega 2022, 7, 11217−11225

Bacterial-Cellulose for Highly-Efficient Capacitive Deionization. *Carbon* **2018**, *130*, 377−383.
(36) An, M.; Du, C.; Du, L.; Sun, Y.; Wang, Y.; Chen, C.; Han, G.; Yin, G.; Gao, Y. Phosphorus-Doped Graphene Support to Enhance Electrocatalysis of Methanol Oxidation Reaction on Platinum Nanoparticles. *Chem. Phys. Lett.* **2017**, *687*, 1−8.
(37) An, M.; Du, L.; Du, C.; Sun, Y.; Wang, Y.; Yin, G.; Gao, Y. Pt Nanoparticles Supported by Sulfur and Phosphorus Co-Doped Graphene as Highly Active Catalyst for Acidic Methanol Electrooxidation. *Electrochim. Acta* **2018**, *285*, 202−213.
(38) Hu, M.; Yao, Z.; Li, L.; Tsou, Y. H.; Kuang, L.; Xu, X.; Zhang, W.; Wang, X. Boron-Doped Graphene Nanosheet-Supported Pt: A Highly Active and Selective Catalyst for Low Temperature H_2-SCR. *Nanoscale* **2018**, *10*, 10203−10212.
(39) Gu, J.; Zhang, Z.; Ding, L.; Huang, K.; Xue, N.; Peng, L.; Guo, X.; Ding, W. Platinum Nanoparticles Encapsulated in HZSM-5 Crystals as an Efficient Catalyst for Green Production of *p*-Aminophenol. *Catal. Commun.* **2017**, *97*, 98−101.
(40) Deshpande, A.; Figueras, F.; Kantam, M. L.; Ratnam, K. J.; Reddy, R. S.; Sekhar, N.S. Environmentally Friendly Hydrogenation of Nitrobenzene to *p*-Aminophenol Using Heterogeneous Catalysts. *J. Catal.* **2010**, *275*, 250−256.
(41) Wang, S.; Wang, Y.; Gao, Y.; Zhao, X. Preparation of SAPO-5 and Its Catalytic Synthesis of *p*-Aminophenol. *Chin. J. Catal.* **2010**, *31*, 637−644.
(42) Quartarone, G.; Ronchin, L.; Tosetto, A.; Vavasori, A. New Insight on the Mechanism of the Catalytic Hydrogenation of Nitrobenzene to 4-Aminophenol in CH_3CN-H_2O-CF_3COOH as a Reusable Solvent System. Hydrogenation of Nitrobenzene Catalyzed by Precious Metals Supported on Carbon. *Appl. Catal., A* **2014**, *475*, 169−178.
(43) Wang, S.; He, B.; Wang, Y.; Zhao, X. MgAPO-5-Supported Pt-Pb-Based Novel Catalyst for the Hydrogenation of Nitrobenzene to *p*-Aminophenol. *Catal. Commun.* **2012**, *24*, 109−113.
(44) Sheng, Y.; Wu, B.; Ren, J.; Wang, X.; Zou, X.; Lu, X. Efficient and Recyclable Bimetallic Co-Cu Catalysts for Selective Hydrogenation of Halogenated Nitroarenes. *J. Alloys Compd.* **2022**, *897*, 163143.
(45) Shimizu, K. I.; Miyamoto, Y.; Satsuma, A. Size- and Support-Dependent Silver Cluster Catalysis for Chemoselective Hydrogenation of Nitroaromatics. *J. Catal.* **2010**, *270*, 86−94.
(46) Zhang, J.; Wang, L.; Shao, Y.; Wang, Y.; Gates, B.; Xiao, F. Product Selectivity Controlled by Steric Adsorption in Zeolite Micropores over a Pd@Zeolite Catalyzed Hydrogenation of Nitroarene. *Angew. Chem.* **2017**, *129*, 9879−9883.
(47) Combita, D.; Concepción, P.; Corma, A. Gold Catalysts for the Synthesis of Aromatic Azocompounds from Nitroaromatics in One Step. *J. Catal.* **2014**, *311*, 339−349.

https://doi.org/10.1021/acsomega.2c00093
ACS Omega 2022, 7, 11217−11225